American Mineralogist, Volume 84, pages 374–383, 1999

The high-pressure, single-crystal elasticity of pyrope, grossular, and andradite

PAMELA G. CONRAD,[1,*] CHANG-SHENG ZHA,[2] HO-KWANG MAO,[1] AND RUSSELL J. HEMLEY[1]

[1]Geophysical Laboratory and Center for High Pressure Research, Carnegie Institution of Washington, 5251 Broad Branch Road, N.W., Washington, D.C. 20015-1305, U.S.A.
[2]Cornell High Energy Synchrotron Source, Cornell University, Ithaca, New York 14853, U.S.A.

ABSTRACT

High-pressure Brillouin scattering experiments were conducted on three natural, single-crystal garnets with near end-member compositions: pyrope ($Mg_3Al_2Si_3O_{12}$), grossular ($Ca_3Al_2Si_3O_{12}$), and andradite ($Ca_3Fe^{3+}{}_2Si_3O_{12}$). Acoustic velocities of the samples were measured from the samples at pressures to 10 GPa in a diamond-anvil cell with a methanol-ethanol-water pressure medium. Elastic stiffness constants (C_{ij}) and their pressure dependencies ($\partial C_{ij}/\partial P$) were calculated, as were aggregate elastic moduli (K_S and G) and their respective pressure derivatives. The Cauchy relations changed with pressure for both grossular and andradite, suggesting that assuming these are constant is not valid for extrapolation to high pressures for these and possibly other minerals. The variation in $\partial K_S/dP$ and $\partial G/\partial P$ was sensitive to composition and required a complex mixing model for extrapolation of end-member elasticity values from garnets of intermediate compositions.

INTRODUCTION

The elastic properties of the Earth's deep interior are increasingly well-resolved by seismology, providing investigators with a foundation on which to base compositional models of the interior. Such models are dependent, however, upon a detailed understanding of the pressure-temperature dependence of the elastic properties of candidate minerals and rocks.

Garnet is considered an important constituent in the Earth's upper mantle, but its modal amount is debated. In the pyrolite model (Ringwood 1975), the mantle is chemically homogeneous between upper and lower mantle, whereas piclogite models (Bass and Anderson 1984; Anderson and Bass 1986) require some chemical stratification with the lower mantle more iron and silica rich than the upper mantle. Both of these models feature garnet as an important mineral with transition zone abundances ranging from 20% for pyrolite to 50% for piclogite (Anderson and Bass 1986; Ita and Stixrude 1992). Garnet, $\{X\}_3[Y]_2(Z)_3O_{12}$, accommodates various chemical substitutions, suggesting that mantle species could be chemically diverse. Because chemical substitution at octahedral and triangular dodecahedral sites changes relative bond lengths and angles, the affected polyhedra may have altered elastic properties as well. This study used Brillouin spectroscopy at pressure to obtain elastic stiffness constants of single crystals of three natural granets (pyrope, grossular, and andradite) and inferred compositional dependence of elastic properties and their pressure derivatives.

Acoustic velocities can be directly measured with several different methods. Brillouin scattering is an optical method involving the inelastic scattering of light by interaction with acoustic phonons in a fluid or solid, which was first applied to mantle minerals at ambient conditions by Weidner (1975) and to minerals at high pressures in the diamond-anvil cell by Shimizu et al. (1982). The thermally generated phonons scatter monochromatic light of wavelength, λ_0, and frequency, ν_0, at an angle, α, in such a way that the Bragg condition, $\lambda_0 = 2n\Lambda \sin(\alpha/2)$, is satisfied, where Λ is the phonon wavelength. Frequency of the phonon, ν_s can be described by the Bragg equation as well: $\nu_s = 2\nu_0(v/c)n \sin(\alpha/2)$, where n is the refractive index and c the velocity of light in a vacuum. The frequency of the scattered light is Doppler shifted, resulting in the Brillouin doublet, given by $\nu_0 \pm \nu_s = \nu_0 \pm 2\nu_0(v/c)n \sin(\alpha/2)$. Shimizu and Sasaki (1992) demonstrated the feasibility of collecting a full set of sound velocity data from cubic crystals within a single plane. Zha et al. (1996) successfully determined a complete set of elastic stiffness constants with velocity data collected from a single-crystal forsterite [111] platelet. The feasibility of using a platelet (i.e., measurement in a single plane of a crystal) to recover Brillouin scattering data is crucial for high-pressure experiments because of the limited optical access of the diamond-anvil cell. Zha et al. (1996) also did Monte Carlo simulations to determine the reliability of C_{ij} data collected from single plane velocity data (again, the orthorhombic forsterite) and found that longitudinal and shear moduli were within $\pm 5\%$ of the starting values in more than 95% of the simulations, although off-diagonal moduli (C_{12}, C_{13}, and C_{23}) had a somewhat larger error, up to $\pm 10\%$ of starting values. Ultimately,

* Present address: Jet Propulsion Lab, Caltech, Mailstop 183-301, Pasadena, California 91109, U.S.A.
E-mail: conrad@jpl.nasa.gov

0003–004X/99/0003–0374$05.00

TABLE 1. Garnet compositions

Pyrope*		Grossular		Andradite	
Oxide	Cation total	Oxide	Cation total	Oxide	Cation total
SiO_2	3.020	SiO_2	2.99	SiO_2	3.04
TiO_2	0.001	TiO_2	0.02	TiO_2	0.00
Al_2O_3	2.014	Al_2O_3	1.97	Al_2O_3	0.12
FeO	0.099	FeO	0.01	Fe_2O_3	1.83
MnO	0.001	MnO	0.01	MnO	0.04
MgO	2.781	MgO	0.04	MgO	0.00
CaO	0.058	CaO	2.95	CaO	2.96
Total	7.973	Total	7.99	Total	7.99

Notes: Water content was determined by IR spectroscopy: pyrope and andradite were essentially anhydrous at 0.0002 wt% (Rossman et al. 1989) and 0.001 wt% (Lu, R., personal communication, 1997), respectively. Grossular contained 0.18 wt% water (sample 771 from Rossman and Aines 1991).

* Dora Maira Massif Western Alps.

TABLE 2. Crystallographic data

	Pyrope	Grossular	Andradite
Lattice parameter, Å	11.466	11.849	12.048
Unit–cell volume, Å^3	1507.425	1663.59	1748.80
Density, g/m^3	3.582	3.60	3.84

Note: All of the garnets are cubic ($Ia\bar{3}d$).

the simulations showed that aggregate compressional and shear velocities were within 1% of calculated values from the known set of elastic stiffness constants, despite the somewhat large scatter in the off-diagonal C_{ij} values.

Experimental procedures

The optical system for the high-pressure Brillouin scattering experiments is described elsewhere (Zha et al. 1996). The principal components are a six-pass Sandercock-type interferometer (Mock et al. 1987) and a single-frequency, argon-ion laser with integral etalon for the excitation source. A 514.5 nm wavelength beam was used here.

High crystal quality and careful preparation of parallel crystal surfaces are crucial for Brillouin scattering experiments to prevent scatter due to surface imperfections from overwhelming the weak signal. All crystals in this study were compositionally homogeneous on the basis of both optical and electron microprobe analysis (EMPA). Neither the pyrope nor the grossular crystals exhibited any detectable birefringence; the andradite showed a first-order cream color birefringence under crossed polars in a 700 μm thick sample. Elemental analyses were obtained with EMPA on a JEOL 8000 instrument; the compositions are reported in Table 1. Crystallographic data are in Table 2. All three of the crystals were broken from natural samples that had previously been examined by infrared spectroscopy (Rossman et al. 1989; Rossman and Aines 1991; Lu 1997, personal communication).

Equant single crystals, approximately 1000 μm × 900 μm × 900 μm, were oriented with X-ray precession photography and subsequently polished into platelets with a 0.3 μm finish on both sides by abrading parallel [110] faces to a thickness, t, of 13 μm for the pyrope and parallel [100] faces to $t \sim 15$ μm for the grossular and andradite crystals. The polished crystals were broken into several smaller pieces; final samples were approximately square with edges <75 μm. The use of a piston-cylinder polishing jig minimized errors in parallelism to within 0.1° (Zha et al. 1996). This is important because curvature of the sample surface can introduce error in the velocity measurement.

A modified version of the Merrill-Bassett diamond-anvil cell (Mao and Bell 1980) was used (Fig. 1). The large conical opening on either side of the symmetrical cell allows light to be collected at forward-scattering angles ≥90° and back-scattering angles ≤45°, the angle referring to that between incident and scattered beam. Forward scattering geometries are ≥90°. Such a wide conical hole significantly weakens the tungsten carbide seat. Therefore, two of the experiments used seats with narrower optical access cones (approximately 65°). This reduction necessitated changing the scattering geometry of the experiment, resulting in a smaller Brillouin shift. The advantage, however, was the ability to achieve hydrostatic conditions at higher pressures without sacrificing the ability to rotate the sample through several crystallographic positions relative to the axis of the incident beam.

A stainless steel gasket was pre-compressed between the anvils to a thickness of 50 μm. Drilling generated a 200 μm diameter sample chamber. The single-crystal samples were repeatedly cleaned, first with acetone, then several times with ethanol to remove any debris that might absorb the laser light, potentially react with the pressure medium, or heat the sample.

The sample was loaded in the center of the gasket hole, flat against the piston diamond culet, as determined by

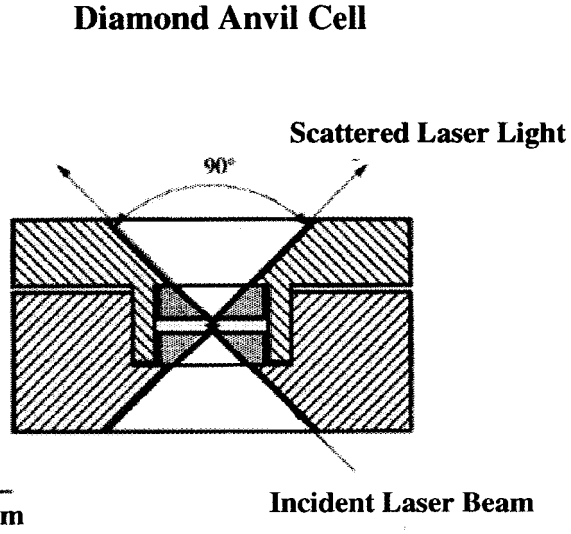

FIGURE 1. The diamond-anvil cell showing the 90° minimum forward scattering angle limitation.

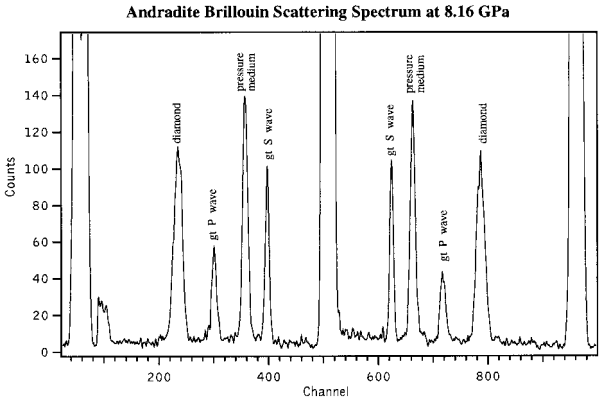

FIGURE 2. An example of a raw Brillouin scattering spectrum. The large peaks in the center and at the extremes of the X axis are the Rayleigh-scattered light. The channel numbers correspond to different frequencies of the scattering peaks.

optical interference. This method effectively controlled alignment error between sample and diamond to <0.3°, which limits the contribution to errors in sound velocity measurement to ≤0.9% (Zha et al. 1996).

A few small grains of ruby were positioned about the garnet for pressure calibration (e.g., Mao et al. 1986). The Brillouin scattering system was equipped with a microscope-optical fiber-spectrograph apparatus for in situ monitoring of pressure with the ruby fluorescence system. Pressure was monitored before, during, and after all experiments. The pressure transmitting medium, a 16:3:1 mixture of methanol-ethanol-water, freezes above 10 GPa (Piermarini et al. 1973); therefore, experiments were limited to 10 GPa to ensure hydrostatic conditions. Crystallographic orientation of the sample with respect to the cell was determined using a precession camera with the X-ray beam parallel to the load axis of the diamonds. Knowledge of the orthogonal crystallographic axes helped to ascertain directions of phonon propagation, which were varied by rotating the cell in a chi circle of an x-y-z stage.

Symmetrical, forward-scattering geometry with a thin crystal platelet allowed measurement of acoustic velocity without knowing the index of refraction. This advantage outweighs the stronger relative Brillouin signal that can be achieved with a backscattering geometry. All three elastic constants (C_{11}, C_{12}, and C_{44}) could be determined from velocity measurements in only two crystallographic orientations within the [100] or [110] planes of the platelet.

The interferometer mirror spacing was 3.8 mm for all experiments. For pyrope, the scattering angle was 90°. For grossular and andradite, the scattering angle was changed to 120° to test the feasibility of accommodating the limitations imposed by diamond-anvil cell seats with narrower conical windows (67°). Figure 2 shows an example of a Brillouin scattering spectrum at pressure.

RESULTS AND DISCUSSION

Cubic structures require only three independent stiffness constants to describe completely their elastic behavior, C_{11}, C_{12}, and C_{44}. Even cubic crystals are not necessarily acoustically isotropic. Acoustic velocities with directional cosines y_1, y_2, y_3 are oriented with respect to crystallographic axes and related to the elastic constants by the Christoffel equation:

$$det|\Gamma_{ij} - \rho V^2\delta_{ij}| = 0$$

where Γ_{ij} is the Kelvin-Christoffel stiffness, a quadratic

TABLE 3. Pyrope acoustic velocities

XTAL direction	N_X	N_Y	N_Z	v_p obs (km/s)	v_p calc (km/s)	Ratio calc/obs	v_s obs (km/s)	v_s calc (km/s)	Ratio calc/Obs
				3.38 GPa*					
100	−0.0000	0.0000	1.0000	9.26	9.27	1.00	5.10	5.09	1.00
	0.1228	−0.1228	0.9848	9.22	9.27	1.00	5.11	5.10	1.00
	0.2418	−0.2418	0.9397	9.24	9.26	1.00	5.09	5.10	1.00
	0.3536	−0.3536	0.8660	9.24	9.24	1.00	5.14	5.11	0.99
	0.4545	−0.4545	0.7660	9.27	9.23	1.00	5.13	5.12	1.00
	0.5417	−0.5417	0.6428	9.30	9.23	0.99	5.14	5.13	1.00
	0.6124	−0.6124	0.5000	9.29	9.23	0.99	5.13	5.13	1.00
	0.6645	10.6645	0.3420	9.30	9.23	0.99	5.13	5.11	1.00
	0.6964	−0.6964	0.1736	9.18	9.23	1.01	5.04	5.10	1.01
110	0.7071	−0.7071	−0.0000	9.13	9.24	1.01	5.06	5.09	1.01
				6.53 GPa†					
100	−0.0000	0.0000	1.0000	9.39	9.41	1.00	5.22	5.23	1.00
110	0.7071	−0.7071	−0.0000	9.42	9.39	1.00	5.27	5.23	0.99
				8.75 GPa‡					
100	−0.0000	0.0000	1.0000	9.53	9.52	1.00	5.24	5.25	1.00
110	0.7071	−0.7071	−0.0000	9.53	9.52	1.00	5.24	5.24	1.00

Notes: Pyrope velocity was measured in several different crystallographic directions with incident beam normal to the [110] face of the crystal. The root mean square (RMS) misfit of the observed to calculated velocities is shown for each pressure. N_X, N_Y, and N_Z are the directional cosines of the orthogonally propagating acoustic waves.

* v_p RMS misfit = 0.059; v_s RMS misfit = 0.026.

† v_p RMS misfit = 0.027; v_s RMS misfit = 0.032.

‡ v_p RMS misfit = 0.04; v_s RMS misfit = 0.039.

function of the directional cosines; $\delta_{ik} = 1$ if i = k and $\delta_{ik} = 0$ if i ≠ k. For a cubic crystal, the Γ_{ij} values (Every 1980) are:

$$\Gamma_{11} = y_1^2C_{11} + y_2^2C_{44} + y_3^2C_{44}$$

$$\Gamma_{22} = y_1^2C_{44} + y_2^2C_{11} + y_3^2C_{44}$$

$$\Gamma_{33} = y_1^2C_{44} + y_2^2C_{44} + y_3^2C_{11}$$

$$\Gamma_{12} = y_1y_2(C_{12} + C_{44})$$

$$\Gamma_{23} = y_2y_3(C_{12} + C_{44})$$

$$\Gamma_{13} = y_1y_3(C_{12} + C_{44})$$

The Christoffel equation has three roots, which correspond to the orthogonally related longitudinal and transverse acoustic waves. In the laboratory, measured velocities can be inverted to a set of best-fit elastic moduli by iterative least-squares adjustment, then measured, and calculated velocities can be compared. Cubic crystals have special directions in which purely longitudinal or transverse phonons may be measured: $\rho v_p^2 = C_{11}$ and $\rho v_s^2 = C_{44}$ in the [100] crystallographic direction. In the [110] direction, $2\rho v_p^2 = (C_{11} + C_{12} + 2C_{44})$ and $2\rho v_s^2 = (C_{11} - C_{12})$. In other crystallographic directions, it is not possible to measure independently the acoustic phonons. Therefore, the acoustic velocities were measured in the special directions. Pyrope velocities (Table 3) were initially measured over ten different crystallographic directions at 3.38 GPa (Fig. 3) to characterize the degree of acoustic anisotropy. At subsequent pressures, velocity was measured six times in the [100] direction with [110] normal to the incident laser beam and six times in the [110] direction, the special crystallographic directions that result in values for all three elastic constants.

For the grossular and andradite experiments, the velocities were initially measured in ten different directions at the lowest pressures (Fig. 3) to characterize the amount of seismic anisotropy; subsequent measurements were taken six times each in the [100] and [110] directions at each pressure (Tables 4 and 5). The root mean square (RMS) deviations between observed and calculated velocities from a best fit set of elastic stiffness constants (C_{ij}) ranged from 0.0001 to 0.09 km/s.

C_{ij} were calculated by inverting the velocity data with a non-linear, least squares method. This method determined a best fit set of elastic stiffness constants by minimizing errors between observed velocities and a set of calculated velocities from a trial set of elastic constants by solution of the Christoffel equation. The experimental precision of the observed velocity measurements was assumed to be 1%, analysis of potential contributions to this margin of error can be found in Zha et al. (1996). The C_{ij} values and uncertainties (1σ) are given in Table 6. The behavior of the elastic stiffness constants with increasing pressure is shown in Figure 4. Pyrope values at ambient conditions were taken from O'Neill et al. (1991), the grossular and andradite values from Bass (1986, 1989).

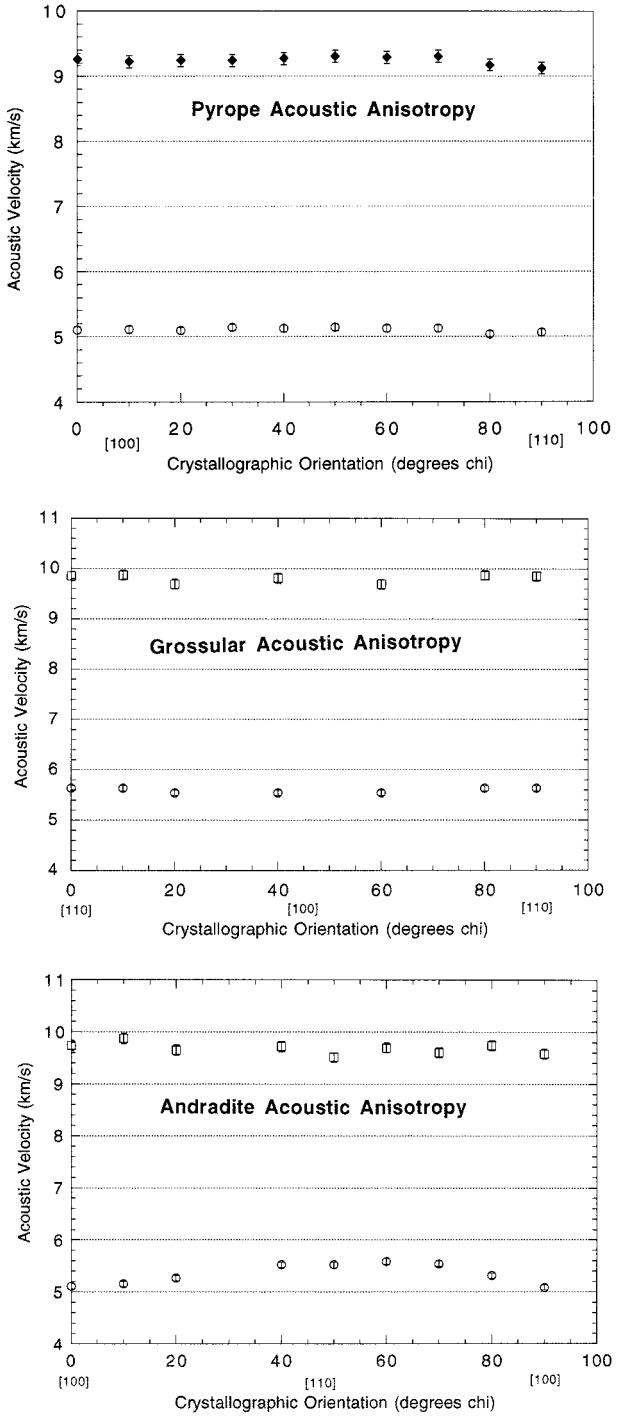

FIGURE 3. Acoustic velocity measured in several different crystallographic directions. All samples are at 3.5 GPa. Error bars represent ±1% of the measured values. All three compositions were isotropic.

The samples from the aforementioned Brillouin scattering studies at ambient conditions have compositions very close (the pyrope was identical), including water content, to the samples used here.

TABLE 4. Grossular acoustic velocities

XTAL direction	N_x	N_Y	N_Z	v_p obs (km/s)	v_p calc (km/s)	Ratio calc/obs	v_s obs (km/s)	v_s calc (km/s)	Ratio calc/Obs
				1.6 GPa*					
[100]	−0.0000	1.0000	−0.0000	9.49	9.42	0.99	5.54	5.61	1.01
[110]	−0.000	0.7660	0.6428	9.46	9.47	1.00	5.52	5.53	1.00
				3.5 GPa†					
[100]	−0.0000	1.0000	−0.0000	9.74	9.68	0.99	5.59	5.51	0.99
[110]	−0.000	0.7660	0.6428	9.67	9.59	0.99	5.52	5.51	1.00
				6.95 GPa‡					
[100]	−0.0000	1.0000	−0.0000	9.85	9.79	0.99	5.63	5.62	1.01
[110]	−0.000	0.7660	0.6428	9.81	9.83	1.00	5.54	5.54	1.00
				7.7 GPa§					
[100]	−0.0000	1.0000	−0.0000	9.81	9.86	0.99	5.70	5.59	1.01
[110]	−0.000	0.7660	0.6428	9.94	9.92	1.00	5.50	5.48	1.00
				10 GPa‖					
[100]	−0.0000	1.0000	−0.0000	9.49	9.42	0.99	5.54	5.61	1.01
[110]	−0.000	0.7660	0.6428	9.46	9.47	1.00	5.52	5.53	1.00

Notes: All velocities were measured with incident beam normal to the [100] surface of the crystal. Each velocity measurement is the mean of six measurements in a given orientation. N_x, N_Y, and N_Z are the directional cosines of the propagating acoustic waves. Root mean square (RMS) errors between observed calculated velocities are as shown.

* v_p RMS misfit = 0.09; v_s RMS misfit = 0.06.
† v_p RMS misfit = 0.05; v_s RMS misfit = 0.08.
‡ v_p RMS misfit = 0.08; v_s RMS misfit = 0.03.
§ v_p RMS misfit = 0.08; v_s RMS misfit = 0.07.
‖ v_p RMS misfit = 0.04; v_s RMS misfit = 0.13.

Calculation of the aggregate elastic moduli, K_S and G, from the elastic stiffness constants at each pressure (Table 7; Fig. 5) reveal the pressure derivatives $\partial Ks/\partial P$ and $\partial G/\partial P$ (Table 7). The adiabatic bulk modulus is given by $K_S = (C_{11} + 2C_{12})/3$ for a cubic crystal. The shear modulus for an aggregate is approximated from the single crystal elastic stiffness constants by various schemes (Watt et al. 1976).

The garnet effective shear moduli were calculated with Voigt-Reuss-Hill (VRH) averaging (Table 7). One Hashin-Shtrikman calculation (H-S) was made for each composition to be certain that the VRH average did not fall outside the H-S bounds, as reported once before. The H-S results were virtually identical to the VRH average.

Comparison with previous work

The elastic stiffness constants and aggregate elastic moduli calculated from the observed acoustic velocities extrapolate backward in good agreement (<1%) to the ambient values of O'Neill et al. (1991) and Bass (1986, 1989) within the experimental uncertainties. The C_{44} value for andradite was an exception with the measured value exceeding the Bass value by 3.7%. This slight disagreement is of minimal concern because of the close

TABLE 5. Andradite acoustic velocity

XTAL direction	N_x	N_Y	N_Z	v_p obs (km/s)	v_p calc (km/s)	Ratio calc/obs	v_s obs (km/s)	v_s calc (km/s)	Ratio calc/Obs
				2.8 GPa*					
	−0.0000	1.0000	−0.0000	9.05	9.05	1.00	5.09	5.14	1.01
[110][100]	−0.000	0.7660	0.6428	8.99	9.02	1.00	5.22	5.16	0.99
				4.7 GPa†					
[100]	−0.0000	1.0000	−0.0000	9.44	9.44	1.0	5.24	5.28	1.01
[110]	−0.000	0.7660	0.6428	9.42	9.42	1.0	5.33	5.28	0.99
				6.4 GPa‡					
[100]	−0.0000	1.0000	−0.0000	9.56	9.56	1.0	5.38	5.39	1.00
[110]	−0.000	0.7660	0.6428	9.52	9.52	1.0	5.41	5.39	0.99
				8.2 GPa§					
[100]	−0.0000	1.0000	−0.0000	9.74	9.74	1.0	5.51	5.52	1.0
[110]	−0.000	0.7660	0.6428	9.72	9.72	1.0	5.52	5.51	1.0
				9.6 GPa‖					
[100]	−0.0000	1.0000	−0.0000	9.88	9.84	0.99	5.68	5.66	1.0
[110]	−0.000	0.7660	0.6428	9.79	9.84	1.01	5.64	5.66	1.0

Notes: All velocities were measured with incident beam normal to the [100] surface of the crystal. Each velocity measurement is from a least squares fit of six measurements in a given orientation. N_x, N_Y, and N_Z are the directional cosines of the propagating acoustic waves. The root mean square (RMS) errors are shown.

* v_p RMS misfit = 0.0001; v_s RMS misfit = 0.07.
† v_p RMS misfit = 0.004; v_s RMS misfit = 0.02.
‡ v_p RMS misfit = 0.0001; v_s RMS misfit = 0.02.
§ v_p RMS misfit = 0.0001; v_s RMS misfit = 0.06.
‖ v_p RMS misfit = 0.004; v_s RMS misfit = 0.06.

TABLE 6. Elastic stiffness constants

Pressure (GPa)	C_{11}	C_{12}	C_{44}
		Pyrope	
0.0001*	297.6(5)	109.8(6)	92.7(7)
3.38	313.8(3)	119.8(3)	94.8(1)
6.53	328.7(7)	122.8(15.0)	101.5(2)
8.75	339.7(4)	133.6(3)	103.1(2)
		Grossular	
0.0001†	321.7	91.4	104.6
1.6	322.25(3)	100.68(3)	114.34(2)
3.5	343.96(5)	108.66(11)	111.56(1)
6.95	358.18(4)	129.00(5)	118.02(2)
7.7	364.41(3)	139.20(4)	117.20(2)
10.0	384.57(4)	145.56(5)	125.84(2)
		Andradite	
0.0001‡	289(2)	92(2)	85(1)
2.8	320.6(6)	105.47(15)	103.77(2)
4.7	351.82(7)	105.57(12)	106.95(2)
6.53	364.29(7)	104.27(3)	116.01(2)
8.2	382.66(6)	118.78(12)	122.26(2)
9.56	400.00(6)	114.68(12)	125.0(2)

Notes: Parenthetical uncertainties represent 1 standard deviation.
* O'Neill et al. 1991.
† Bass 1989.
‡ Bass 1986.

agreement between the aggregate elastic moduli of the different experiments. The agreement with ambient values confirms the reliablility of elastic stiffness constants obtained from velocity data for only two crystallographic orientations from a platelet within a diamond-anvil cell.

To date, only a few other high-pressure elasticity studies exist in which the complete set of elastic constants were determined from single-crystal samples. Webb (1989) applied ultrasonic interferometry to 3 GPa on a single-crystal garnet with composition $Py_{0.62}Alm_{0.36}Gr_{0.02}$. Acoustic velocity data were collected from a $Py_{51.6}Alm_{31.7}Gr_{15.8}Sp_{0.9}$ single-crystal sample by impulsive stimulated scattering (Chai et al. 1997). Webb (1989) and Chai et al. (1997) compared their results with a combination of values extrapolated from static compression experiments and the ambient pressure Brillouin scattering data of O'Neill et al. (1991) and Bass (1989). In fact, many garnet elasticity studies have involved the extrapolation of data from complex composition garnets to end-member values. This approach makes direct comparison of experimental data difficult, because selection of the composition-elasticity model may introduce systematic errors that prevent accurate comparisons. Chai et al. (1997) used the Isaak and Graham (1976) and Babuska et al. (1978) mixing models wherein the C_{ij} of any solid solution are related linearly to the mole fraction of the end-members. This mixing model gives end-member extrapolations of bulk and shear moduli to be systematically lower than those predicted by weighted superposition of the Bass (1989) and O'Neill et al. (1991) end-member values (with which the present study is in agreement). Extrapolations of the elastic moduli of mixed compositions to end-member compositions should be avoided, because if each component of a complex garnet composition has a different K', there will certainly be disagreement

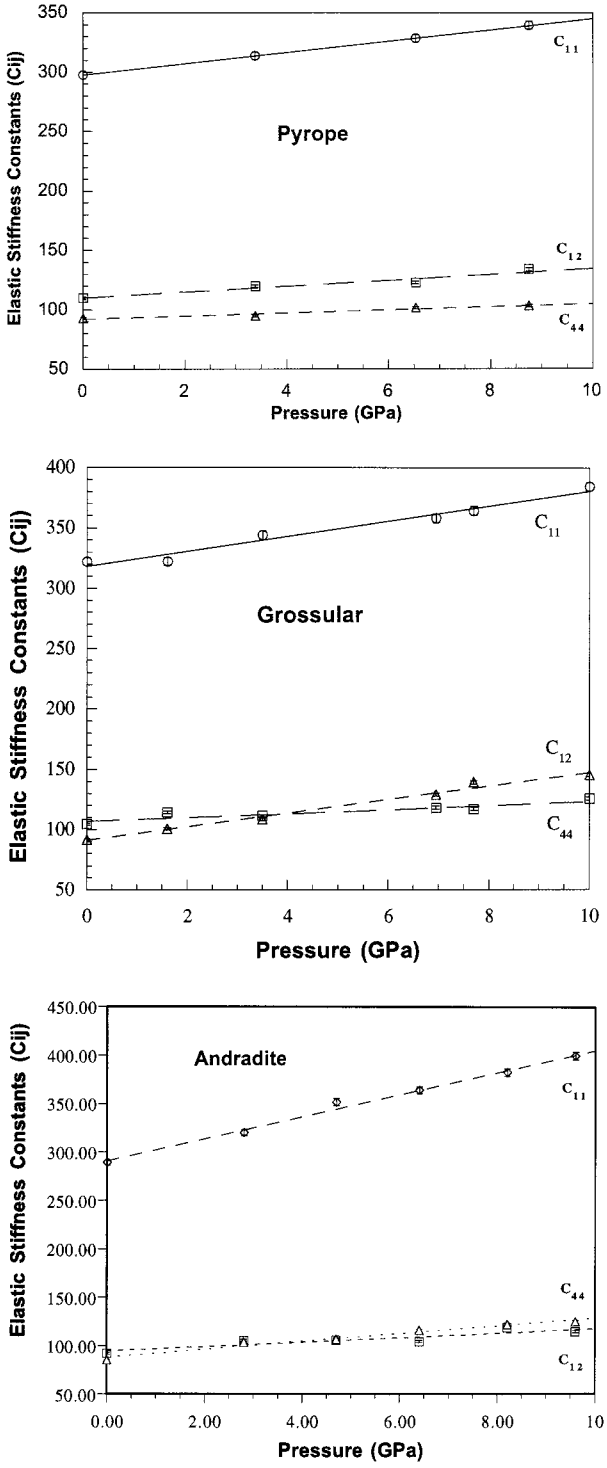

FIGURE 4. The pressure dependence of the elastic stiffness (C_{ij}) constants. Ambient values are from O'Neill et al. (1991) for pyrope and from Bass (1986, 1989) for andradite and grossular respectively.

TABLE 7. Adiabatic and isothermal bulk moduli.

	K_S GPa	K_T GPa	$\partial K/\partial P$	G* GPa	$\partial G/\partial P$
pyrope	172.73	171.32	3.22	92†	1.4
grossular	166.82	165.68	5.46	108.9‡	1.1
andradite	159.38	158.31	5.85	90§	4.3

Notes: The conversion from adiabatic to isothermal bulk modulus is given by: $K_s = K_T(1 + \gamma\alpha T)$, where γ is the thermodynamic Grüneisen parameter and α is the thermal expansion. Values for these parameters were taken from Anderson and Isaak (1995).

* G is from Voight-Reuss-Hill averaging.

† O'Neill et al. (1991).

‡ Bass (1989).

§ Bass (1986).

between end-member measurements and extrapolations from mixed composition samples. The discrepancy between the Chai et al. (1997) extrapolations and the Bass (1989) and O'Neill et al. (1991) end-member garnet elastic moduli may also be due to other factors. (1) The ferric iron content of the Chai et al. sample was not reported; its stoichiometry was based upon formula recalculation from electron microprobe analysis, a technique that is insensitive to element oxidation states. Given that an andradite component would reduce both bulk and shear modulus, this could be an important factor. (2) Bass (1986) demonstrated that a linear mixing model is not a good approximation for the ugrandite garnets; the models predict too low a bulk modulus for andradite.

Implications for static compression experiments

After converting the adiabatic bulk moduli from the elastic stiffness constants to isothermal values (Table 7), the pressure derivative K_T' can be used to constrain bulk modulus values from static compression experiments. Pyrope has been the subject of nearly a dozen static compression experiments, several ultrasonic measurements, and a few Brillouin scattering experiments (Tables 8 and 9). The range of values for K_T is broad, but many values converge when the K_T' is fixed at 3.22, bringing the static compression data of Levien et al. (1979), Sato et al. (1978), and Leger et al. (1990) into excellent agreement within respective experimental uncertainties (Fig. 6). Grossular static compression experiments are fewer and the K_T' of 5.46 places the work of Weaver et al. (1976) and Olijnyk et al. (1991) in excellent agreement with each other. Andradite has only been the subject of one static compression experiment (Hazen and Finger 1989), and our results are in agreement within the experimental uncertainties.

Several garnet elasticity studies sought to develop composition-elasticity systematics (e.g., Soga et al. 1967; Isaak and Graham 1976; Babuska et al. 1978; Leitner et al. 1981). Although no systematic relations have emerged to predict the behavior of all end-member pyralspites and ugrandites (or all majorites!), the following trends are apparent. (1) Unit-cell volume and bulk modulus are linearly related (Hazen et al. 1994). (2) Substitution of Fe^{2+} for Mg^{2+} in the $\{X\}^{VIII}$ site will increase both K and G. (3) Substitution of Ca^{2+} for Mg^{2+} in the $\{X\}^{VIII}$ site will decrease K and increase G. (4) Substitution of Fe^{3+} for Al^{3+} in the $[Y]^{VI}$ site will result in a decrease of both K and G. (5) Substitution of Fe^{3+} for Al^{3+} in the $[Y]^{VI}$ site results in an increase of $\partial G/\partial P$. (6) The assumption that $\partial K_S/\partial P = 4$ is inappropriate for garnets, as evidenced by

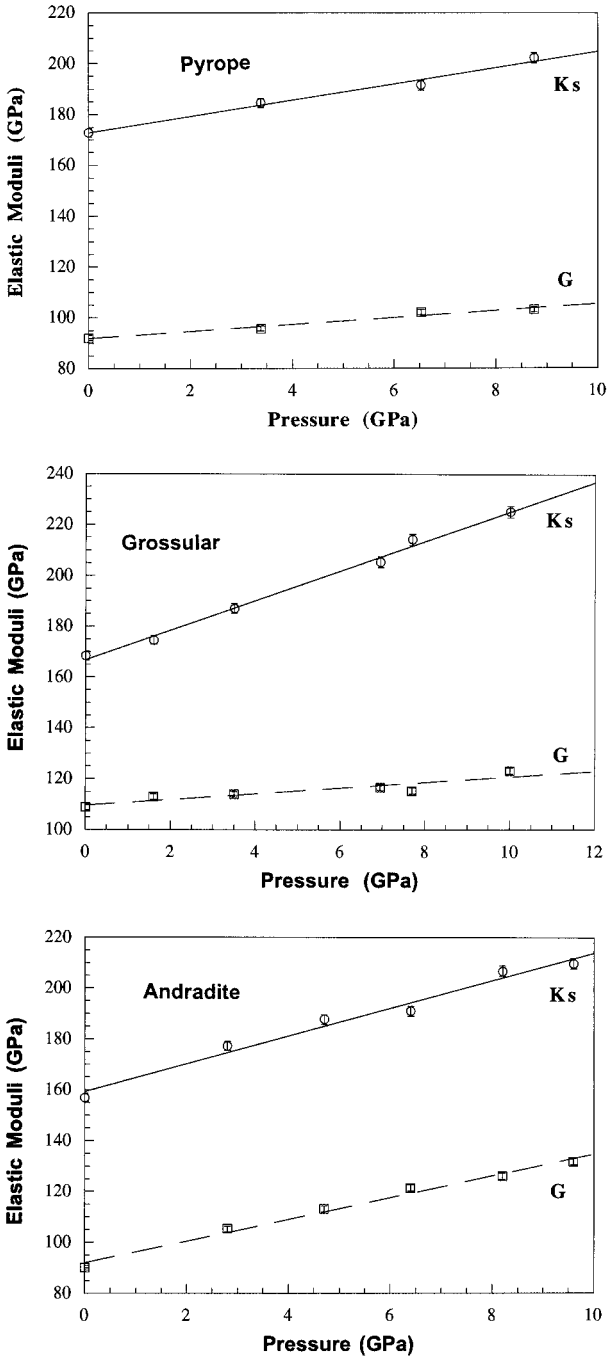

FIGURE 5. Aggregate elastic moduli for all three garnets. Ambient values are from O'Neill et al. (1991) for pyrope and from Bass (1986, 1989) for andradite and grossular.

TABLE 8. Garnet acoustic velocity studies

Reference	Method	Composition	V_p km/s	V_s km/s	C_{11}	C_{12}	C_{44}
Verma (1960)	ultrasonic interferometry	$(Mg_{0.14}Fe_{0.81}Mn_{0.01}Ca_{0.04})_3Al_2Si_3O_{12}$	8.48	4.73	300.8	112	94.4
Soga (1967)	ultrasonic interferometry	$(Mg_{0.21}Fe_{0.76}Ca_{0.03})_3Al_2Si_3O_{12}$	8.53	4.76	302.7	117.3	92.7
Wang and Simmons (1974)	ultrasonic interferometry	$(Fe_{0.46}Mn_{0.54})_3Al_2Si_3O_{12}$	8.48	4.72	308.5	112.3	94.8
Goto et al. (1976)	ultrasonic interferometry	$(Mg_{0.55}Fe_{0.37}Mn_{0.01}Gr_{0.06}$	8.80	4.96	298.84	109.64	94.6
Isaak and Graham (1976)	ultrasonic interferometry	$(Fe_{0.46}Mn_{0.54})_3Al_2Si_3O_2$	8.50	4.72	306.42	117.72	94.35
Bonczar et al. (1977)	ultrasonic interferometry	$(Mg_{0.61}Fe_{0.36}Ca_{0.02})_3Al_2Si_3O_{12}$	8.86	4.96	292.75	109.55	91.60
Leitner et al. (1980)	Brillouin scattering	$Mg_3Al_2Si_3O_{12}$	9.08	5.02	295	117	90
Bass (1986)	Brillouin scattering	$Ca_{2.99}Mg_{0.01}(Fe_{1.92}Al_{0.08})Si_3O_{12}$	8.51	4.85	289	92	85
		$Ca_3Cr_2Si_3O_{12}$	8.6	4.89	304	91	84
Webb (1989)	ultrasonic interferometry	$(Mg_{0.62}Fe_{0.36}Ca_{0.02})_3Al_2Si_3O_{12}$	8.84	4.97	301.4	110.0	94.3
Bass (1989)	Brillouin Scattering	$(Ca_{0.998}Mn_{0.002})_3(Al_{0.992}Fe_{0.008})_2Si_3O_{12}$	9.45	5.39	321.7	91.2	104.6
		$(Mn_{0.948}Fe_{0.05}Ca_{0.002})_3Al_2Si_3O_{12}$	8.59	4.76	309.5	113.5	95.2
O'Neill et al. (1991)	Brillouin Scattering	$(Mg_{0.90}Fe_{0.08}Ca_{0.02})_3Al_2Si_3O_{12}$	9.09	5.07	297.6	109.8	92.7
Chopelas et al. (1996)	*sideband fluorescence	$Mg_3Al_2Si_3O_{12}$	9.16	5.06	–	–	–
Chai et al. (1997)	*ISS	$Py_{51.6}Al_{31.7}Gr_{15.8}Sp_{0.9}$	8.86	4.96	299.1	106.7	93.7
Chen et al. (1997)	GHz ultrasonic interferometry	$Py_{97}Alm_2$	9.05	5.09			
		$Py_{27}Alm_{73}$	8.50				

Notes: All of the experiments shown here are on pyralspite/ugrandite (low-pressure) garnets. Exact compositions have been listed where known.
* Denotes a high pressure experiment.

the high-pressure behavior of the three compositions in the present study.

One consequence may partially resolve the discrepancy between reports of the bulk modulus for a $(Na_2Mg)Si_2Si_3O_{12}$ majorite by Pacalo et al. (1993) from a Brillouin scattering experiment and by Hazen et al. (1994) from a static compression experiment. The Brillouin scattering data indicated a bulk modulus of 173.5 GPa; however, the static compression data indicated a bulk modulus of 191.5 ± 2 GPa with an assumed K' of 4. From the data in the present study, the accommodation of Ca in the distorted dodecahedral (X) site appeared to have a correspondingly large K', nearly 6. This K' value would decrease the static compression K_T value. Other possibilities for the discrepancy were noted by Hazen et al. (1994), such as a possibly incorrect identification of the refractive index for the Na majorite in the Brillouin scattering experiment or a change in compression mechanism with pressure. Although the present study did not involve any majorite samples, inclusion of the Na majorite in this discussion is appropriate because of its similar elastic behavior to grossular and its unusual crystal chemistry: accommodation of Na in the X site (the largest cation thought to fit in this site had been Ca) and the accommodation of Si in the octahedral site. This cubic majorite had an extremely large G equaling 114.7 GPa, the highest value measured for a garnet. As in grossular, $C_{44} > C_{12}$ at ambient conditions. The present study indicates that the relationship between these two values changes with pressure for grossular, becoming equal at

TABLE 9. Garnet static compression studies

Study	Composition	K_T (GPa)	$\partial K_T/\partial P$
Takahashi and Liu (1970)*	$Mg_3Al_2Si_3O_{12}$	190 ± 6	5.45 assumed from Soga (1967)
	$Fe_3Al_2Si_3O_{12}$	168 ± 5	5.45 assumed from Soga (1967)
	$Py_{60}Alm_{31}$	177 ± 6	5.45 assumed from Soga (1967)
	$Py_{22}Alm_{72}$	173 ± 6	5.45 assumed from Soga (1967)
Duba and Olinger (1972)†	$(Mg_{0.57}Fe_{0.28}Ca_{0.15})(Al,Ti)_2Si_3O_{12}$	175.0 ± 2.0	5.45 assumed from Soga (1967)
Weaver et al. (1976)*	$Ca_3Al_2Si_3O_{12}$	174 ± 4	constrained to 4.5
Sato et al. (1978)‡	$Mg_3Al_2Si_3O_{12}$	171 ± 1	1.8 ± 0.7
	$Fe_3Al_2Si_3O_{12}$	175 ± 7	1.5 ± 1.6
Levien et al. (1979)*§	$Mg_3Al_2Si_3O_{12}$	175 ± 1	4.5 ± 0.5
Sawamoto (1987)‖	$MgSiO_3$	177	4.5
Hazen and Finger (1989)*§	$Ca_3Fe_2Si_3O_{12}$	159 ± 2	4 assumed
	$Mg_3Al_2Si_3O_{12}$	179 ± 3	4 assumed
Leger et al. (1990)*	$Mn_3Al_2Si_3O_{12}$	171.8	7.4 ± 1
	$Mg_3Al_2Si_3O_{12}$	175 ± 0.3	3.3 ± 1
	$Ca_3Cr_2Si_3O_{12}$	162	4.7 ± 0.7
Olijnyk et al. (1991)*	$Ca_3Al_2Si_3O_{12}$	167.8 ± 25	6.2 ± 4

Notes: DAC = diamond-anvil cell, XRD = X-ray diffraction. Measurement error is tabulated where available. K_T and $\partial K/\partial P$ are interdependent through the equation of state (Bell et al. 1987).
* DAC, XRD.
† Piston cylinder, in-situ powder XRD.
‡ Cubic anvil, XRD.
§ Single xtal.
‖ Multi-anvil press, XRD.

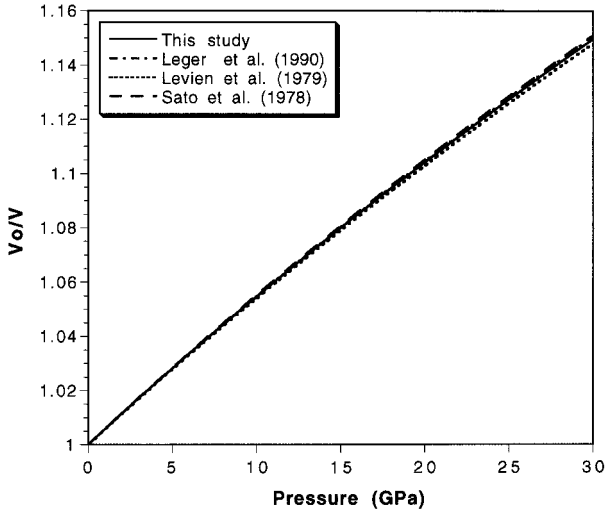

FIGURE 6. A comparison of bulk modulus values for pyrope from static compression experiments where K' is fixed to the value of 3.22 from this study.

around 3 GPa then C_{12} becomes increasingly larger than C_{44} with pressure. Andradite showed the opposite behavior with C_{12} initially larger than C_{44} by a marginal amount. The relationship gradually became inverted at ~4 GPa, with C_{44} becoming increasingly larger than C_{12}. The behavior of the Na majorite C_{44} and C_{12} under pressure would be useful in establishing a relationship between octahedral cation occupancy and elasticity because Na-rich majorite has close to complete ordering of Mg and Si in octahedral sites. Although most elasticity-composition studies have focused upon the X site (Soga 1967; Isaak 1976; Babuska 1978; Leitner 1981), the octahedral site may have a more profound impact on the bulk modulus, as proposed by Hazen et al. (1994). The size of the dodecahedral cation is certainly important because the octahedra share six edges with dodecahedra, and it likely plays a role in determination of individual elastic stiffness constants. If octahedral cation size and valence are the primary factors governing K, the dodecahedral cation size may be an influential factor in K'.

The G' reported for andradite, 4.3, was unusually large and not typical for a silicate. The data exhibited more scatter than the pyrope or grossular data, but the linear fit was quite close with R = 0.994. The C_{12} measurements exhibited the largest differences between Voigt and Reuss values, averaging 0.35 GPa compared with the V-R differences averaging 0.5 GPa for grossular. It would be particularly useful to extend the range of pressures over which the velocities were measured to look for further changes in the behavior of this mode. These data are consistent with the Zha et al. (1996) observation of slightly larger errors in C_{12} measurements than with C_{11} and C_{44} measurements when recovering sound velocity data from a single plane of a crystal platelet.

CONCLUSIONS

This work has demonstrated the feasibility of measuring acoustic velocities multiple times in special crystallographic directions so that diamond-anvil cells with restricted optical access may be used even in higher-pressure experiments. Sound velocities, elastic stiffness constants, and aggregate elastic moduli of pyrope, grossular, and andradite all increased linearly with pressure and acoustic isotropy was maintained throughout the range of pressures studied. The pressure dependency of the elastic moduli (K_S and G) was composition sensitive. C_{44} and C_{12} increased at different rates with pressure, so determination of the Cauchy relation at ambient was not indicative of the high-pressure relations for these garnets.

ACKNOWLEDGMENTS

The authors thank T.S. Duffy (Princeton University) for help with statistical analysis of the data. H. Yang (Geophysical Laboratory) provided help with crystallographic orientation of samples. Samples were kindly provided by K. Kingma, R. Lu, and G.R. Rossman. Helpful suggestions from two anonymous reviewers improved the manuscript, as did the careful eye of Associate Editor A. Chopelas. This work was supported by NSF grant EAR-9526763. Fellowship to P. Conrad supported by the Center for High-Pressure Research and The Carnegie Institution of Washington.

REFERENCES CITED

Anderson, D.L. and Bass, J.D. (1986) Transition region of the Earth's upper mantle. Nature, 320, 321–328.

Babuska, V., Fiala, J., Kumazawa, M., and Ohno, I. (1978) Elastic properties of garnet solid-solution series. Physics of the Earth and Planetary Interiors, 16, 157–176.

Bass, J.D. and Anderson, D.L. (1984) Composition of the upper mantle: geophysical tests of two petrological models. Geophysical Research Letters, 11, 237–240.

Bass, J.D. (1986) Elasticity of uvarovite and andradite garnets. Journal of Geophysical Research, 91, 7505–7516.

———(1989) Elasticity of grossular and spessartite garnets by Brillouin spectroscopy. Journal of Geophysical Research, B, Solid Earth and Planets, 94, 7621–7628.

Chai, M., Brown, J.M., and Slutsky, L.J. (1997) The elastic constants of a pyrope-grossular-almandine garnet to 20 GPa. Geophysical Research Letters, 24, 523–526.

Chen, G., Miletich, R., Mueller, C., and Spetzler, H.A. (1997) Shear and compressional mode measurements with GHz ultrasonic interferometry and velocity-composition systematics for the pyrope-almandine solid-solution series. Physics of the Earth and Planetary Interiors, 99, 273–287.

Chopelas, A., Reichmann, H.J., and Zhang, L. (1996) Sound velocities of five minerals to mantle pressures determined by the sideband fluorescence method. In M.D. Dyar, C. McCammon, and M.W. Schaefer, Eds., Mineral Spectroscopy: A Tribute to Roger G. Burns, p. 229–241. The Geochemical Society, Washington, D.C.

Duba, A. and Olinger, B. (1972) Compression of garnet to 100 kilobars. Journal of Geophysical Research, 77, 2496–2499.

Every, A.G. (1980) General closed form expressions for acoustic waves in elastically anisotropic solids. Physical Review B, 22, 1746–1760.

Goto, T., Ohno, I., and Sumino, Y. (1976) The determination of elastic constants of natural pyrope-almandine garnet by means of rectangular parallelepiped resonance method. Physics of the Earth, 24, 149–158.

Hazen, R.M., Downs, R.T., Conrad, P.G., Finger, L.W., and Gasparik, T. (1994) Comparative compressibilities of majorite-type garnets. Physics and Chemistry of Minerals, 21, 344–349.

Hazen, R.M. and Finger, L.W. (1989) High pressure crystal chemistry of andradite andpyrope: revised procedures for high pressure diffraction experiments. American Mineralogist, 74, 252–359.

Isaak, D.G. and Graham, E.K. (1976) The elastic properties of an almandine-spessartinegarnet and elasticity in the garnet solid solution series. Journal of Geophysical Research, 81, 2483–2489.

Ita, J. and Stixrude, L. (1992) Petrology, elasticity, and composition of the mantle transition zone. Journal of Geophysical Research, 97, 6849–6866.

Leger, J.M., Redon, A.M., and Chateau, C. (1990) Compressions of synthetic pyrope, Spessartine, and uvarovite garnets up to 25 GPa. Physics and Chemistry of Minerals, 17, 161–167.

Leitner, B.J., Weidner, D.J., and Liebermann, R.C. (1981) Elasticity of single crystal pyrope and implications for garnet solid solution series. Physics of the Earth and Planetary Interiors, 22, 111–121.

Levien, L., Prewitt, C.T., and Weidner, D.J. (1979) Compression of pyrope. American Mineralogist, 64, 7–8.

Mao, H.K. and Bell, P.M. (1980) Design and operation of a diamond-window high-pressure cell for the study of single-crystal samples loaded cryogenically. Yearbook Carnegie Institution of Washington, 79, 409–411.

Mao, H.K., Xu, J., and Bell, P.M. Calibration of the ruby pressure gauge to 800 kbar under quasi-hydrostatic conditions. Journal of Geophysical Research, 91, 4673–4676, 1986.

Mock, R., Hillebrands, B., and Sandercock, R. (1987) Construction and performance of a Brillouin scattering set-up using a triple pass tandem Fabry-Perot interferometer. Journal of Physics E: Scientific Instrumentation, 20, 656–659.

O'Neill, B., Bass, J.D., Rossman, G.R., Geiger, C.A., and Langer, K. (1991) Elastic properties of pyrope. Physics and Chemistry of Minerals, 17, 617–621.

Olijnyk, H., Paris, E., Geiger, C.A., and Lager, G.A. (1991) Compressional study of katoite [$Ca_3Al_2(OH_4)^3$] and grossular garnet. Journal of Geophysical Research, 96, 14313–14318.

Pacalo, R.E.G., Weidner, D.J., and Gasparik, T. (1993) Elastic properties of sodium-rich majorite garnet. Geophysical Research Letters, 19, 1895–1898.

Piermarini, G.J., Block, S., and Barnett, J.D. (1973) Hydrostatic limits in liquids and solids to 100 kbar. Journal of Applied Physics, 44, 5377–5382.

Ringwood, A.E. (1975) Composition and petrology of the Earth's mantle, 618 p. McGraw-Hill, New York.

Rossman, G.R. and Aines, R.D. (1991) The hydrous components in garnets: grossular-hydrogrossular. American Mineralogist, 76, 1153–1164.

Rossman, G.R., Berab, A., and Langer, K. (1989) The hydrous component of pyrope from the Dora Maira Massif, Western Alps. European Journal of Mineralogy, 1, 151–154.

Sato, Y., Akaogi, M., and Akimoto, S. (1978) Hydrostatic compression of the synthetic garnets pyrope and almandine. Journal of Geophysical Research, 83, 335–338.

Sawamoto, H. (1987) Phase diagram of $MgSiO_3$ at pressures up to 24 GPa and temperatures up to 2200 °C: phase stability and properties of tetragonal garnet. In M.H. Manghnani and Y. Syono, Eds., High-Pressure Research in Mineral Physics, Geophysical Monograph Series, 39, p. 209–219. American Geophysical Union, Washington, D.C.

Shimizu, H. and Sasaki, S. (1992) High-pressure Brillouin studies and elastic properties of single crystal H_2S grown in a diamond cell. Science, 257, 514–516.

Shimizu, H., Bassett, W.A., and Brody, E.M. (1982) Brillouin-scattering measurements of single-crystal forsterite to 40 kbar at room temperature. Journal of Applied Physics, 53, 620–626.

Soga, N. (1967) Elastic constants of garnet under pressure and temperature. Journal of Geophysical Research, 72, 4227–4234.

Takahashi, T. and Liu, I. (1970) Compression of ferromagnesian garnets and the effect of solid solutions on the bulk modulus. Journal of Geophysical Research, 75, 5757–5766.

Verma, R.K. (1960) Elasticity of some high-density crystals. Journal of Geophysical Research, 65, 757–766.

Wang, H. and Simmons, G. (1974) Elasticity of some mantle crystal structures, 3. spessartite-almandine garnet. Journal of Geophysical Research, 79, 2607–2613.

Watt, J.P., Davies, G.F., and O'Connell, R J. (1976) The elastic properties of composite materials. Reviews of Geophysics and Space Physics, 14, 541–563.

Weaver, J.S., Takahashi, T., and Bass, J. (1976) Isothermal compression of grossular garnets to 250 kbar and the effect of calcium on the bulk modulus. Journal of Geophysical Research, 81, 2475–2482.

Webb, S.L. (1989) The elasticity of the upper mantle orthosilicates olivine and garnet to 3 GPa. Physics and Chemistry of Minerals, 16, 684–692.

Weidner, D.J. (1975) Elasticity of microcrystals. Geophysical Research Letters, 2, 189–192.

Zha, C.S., Duffy, T.S., Downs, R.T., Mao, H.K., and Hemley, R.J. (1996) Sound velocity and elasticity of single crystal forsterite to 16 GPa. Journal of Geophysical Research, 101, 17535–17545.

Manuscript received June 3, 1998
Manuscript accepted October 14, 1998
Paper handled by Anastasia Chopelas